COMPUTATIONS OF THE TRANSIENT MAGNETIC FIELDS, CURRENT DENSITIES AND TEMPERATURE RISES IN THE CERN LITHIUM LENS

A. Ijspeert, P. Sievers
European Organization for Nuclear Research (CERN)
CH-1211 Geneva 23, Switzerland

Summary

Computations of the 3-dimensional, axisymmetric transient magnetic fields and currents inside the CERN-Lithium lens have been made. They allow in particular to study in detail the end fields and the current densities at interfaces between different materials and at locations with abrupt deviations of the current paths where elevated ohmic heating may occur. We present overall pictures of the development in space and time of the transient currents and the temperatures inside the lithium and its complex steel housing, as well as details at its current contacts and its end faces. A result of the field distribution is given in reference 1.

Introduction

The transient magnetic fields and current densities in the CERN-lithium lens have until now been calculated for a simplified model consisting of an infinitely long lens[2,3,4]. The results were used to find the optimum pulse shape and the working point and also to calculate the temperatures and the stresses due to the ohmic heating and the magnetic forces. Phemomena like the end fields or the current densities at the interfaces between different materials where ohmic heating may occur, could not be studied with that model but are also difficult to measure. Therefore, we have investigated these effects with the calculation of a 3-dimensional, axisymmetric model of the lens.

Method of Calculation

Neglecting true charges and wave effects which are much faster than the eddy current distribution, Maxwells equations can be written as follows:

$$\cdot = 0 \qquad (1)$$

$$\cdot = 0 \qquad (2)$$

$$\times = - / t \qquad (3)$$

$$\times = \text{itrue} \qquad (4)$$

where:

$$= \varepsilon \quad \cdot \quad = \mu \qquad = \gamma$$

and ε is the permittivity
μ is the magnetic permeability
γ is the electric conductivity.

Since the lens is axisymmetric, which implies in particular that only the tangential component H_φ of the magnetic field exists, the equations 3 and 4 reduce to:

$$\frac{\mu H_\varphi}{t} = - \frac{E_r}{z} + \frac{E_z}{r} \qquad (5)$$

$$\frac{H_\varphi}{z} = - \gamma E_r \qquad (6)$$

$$\frac{1}{r}\frac{rH_\varphi}{r} = \gamma E_z \qquad (7)$$

The tangential component E_φ of the electric field vanishes.

From these equations, we find:

$$\frac{}{r}\left(\frac{1}{\gamma}\frac{1}{r}\frac{rH_\varphi}{\gamma}\right) + \frac{}{z}\left(\frac{1}{\gamma}\frac{H_\varphi}{z}\right) = \mu\frac{H_\varphi}{t} \qquad (8)$$

where μ is not a function of the time.

A suitable computer program for the calculation of eddy currents is not readily available at CERN. However, by making use of the similarity between electric and thermal field equations, the finite element program DOT[5,6] for nonlinear heat transfer problems can be employed. Equation 8 can be rewritten in one unique variable $rH_\varphi(r,z,t)$ as:

$$r\left(\frac{1}{\gamma}\frac{1}{r}\frac{rH_\varphi}{r}\right) + \frac{}{z}\left(\frac{1}{\gamma}\frac{1}{r}\frac{rH_\varphi}{z}\right) = \frac{\mu}{r}\frac{rH_\varphi}{t} \qquad (9)$$

The structure of this equation is the same as that for 2-dimensional non-stationary heat transport problems in cartesian coordinates. The equivalences are:

Coordinate	x	$= r$
Temperature	$T(x,z,t)$	$= rH_\varphi(r,z,t)$
Thermal conductivity	$\lambda(x)$	$= 1/(\gamma r)$
Specific heat	$\rho c(x)$	$= \mu/r$

where the thermal properties of the material depend on the radius (inhomogeneous material). From the solution of rH_φ one finds the electric field components:

the radial component $E_r = -(1/\gamma r)\ rH_\varphi/\ z$
the axial component $E_z = (1/\gamma r)\ \Gamma H_\varphi/\ r$

When a current pulse supplied from an external source passes through the lens, the boundary conditions consist of known magnetic fields H_φ, defined at any boundary R by the equation:

$$RH_\varphi(t) = I(t)/2\pi$$

where I(t) represents the axial current enclosed within the particular boundary.

The continuity conditions at the interface between two different materials are:

tangential to the boundary: $E_{t1} = E_{t2}$, $H_{t1} = H_{t2}$

normal to the boundary: $\gamma_1 E_{n1} = \gamma_2 E_{n2}$, $\mu_1 H_{n1} = \mu_2 H_{n2}$

These conditions are satisfied as shown in reference 6.

Geometry and Boundary Conditions

The detailed mechanical design of the lens is given in reference 1. The symmetry of the lens allows to consider only a quarter of its structure (Figure 1) limited by the axis and by the symmetry plane. The different materials are characterised by their electric constants, the relative permeability has been taken 1 everywhere and the air has been considered as an electric insulator. Geometrically, a compromise has been made in that the 8 distinct lithium channels which act as current leads in the steel body had to be represented by a complete axially symmetric

cylindrical lithium channel. In addition, the titanium end cover and its steel flange have not been modeled as this appears to be a practically field and current free area.

The boundary conditions are defined by the current pulse and consist of given magnetic fields or gradients as indicated in Figure 1.

The current pulse is a damped half sine pulse with a duration of 600 microseconds:

$$I(t) = I_0 \, e^{-\delta t} \sin \omega t \quad (0 < t < \pi/\omega)$$

where current pulse amplitude I_0 = 721 kA
pulse damping δ = 1750 Hz
pulse duration π/ω = 600 µs

The effective peak value, attained at 240 µsec, is 450 kA.

The skin depth of the different materials at the frequency ω is:

Aluminium 2.9 mm
Stainless Steel 14.8 mm
Lithium 5.3 mm

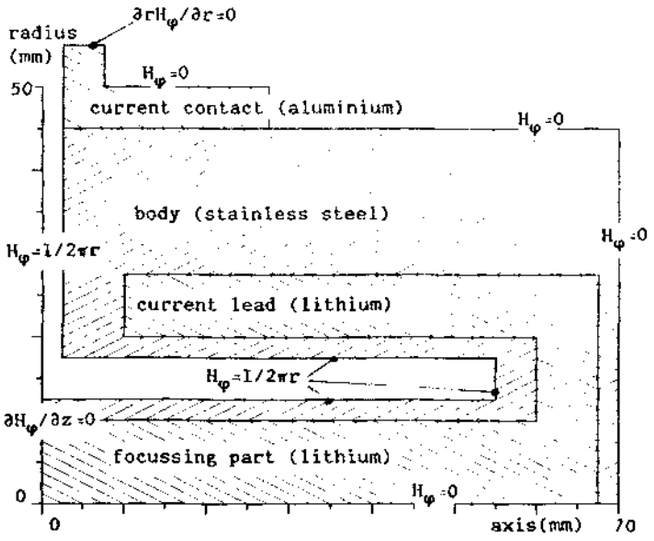

Fig. 1. The model of the lithium lens and the boundary conditions.

Results

Figure 2 shows the current distribution at 4 different instants; in the early beginning of the pulse (Fig. 2a), at the peak of the pulse (Fig. 2b), at the working point 120 µsec. beyond the peak of the pulse where the current density in the central lithium cylinder is most uniform (Fig. 2c), and finally at the

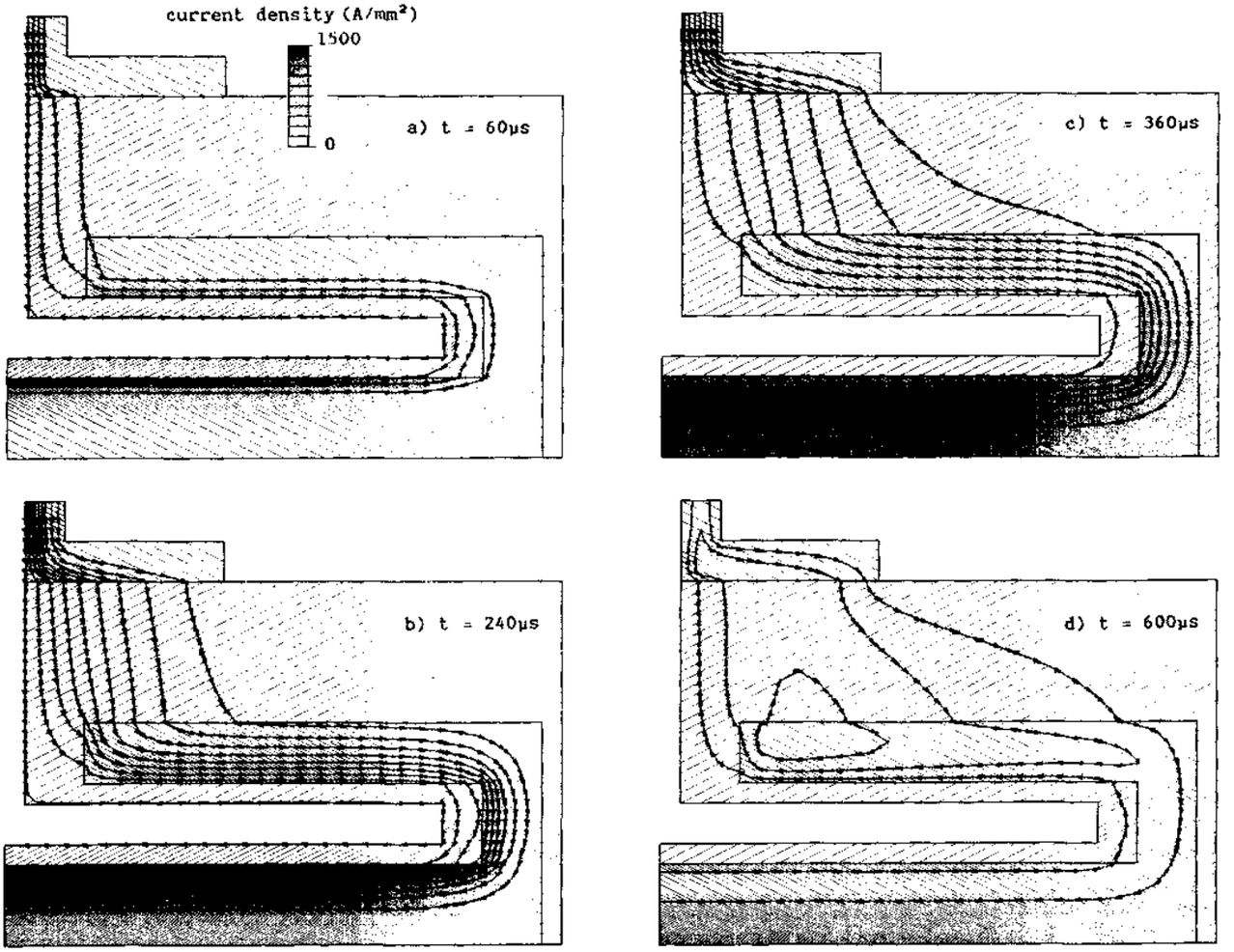

Fig. 2. The current flow in the lithium lens.
50 kA are enclosed between each 2 flow lines, the current density is proportional to the raster density.

end of the pulse (Fig. 2d). The current flux between each two flow lines is 50 kA; however, the line density is not proportional to the current density due to the cylindrical geometry. Therefore, the current density is indicated by means of a raster density. The scales are given in the figure.

During the rise of the pulse the increasing current is gradually diffused from the rim into the body. Beyond the peak of the pulse negative currents are introduced along the boundaries which lead finally to vortex like currents as shown in Figure 2d.

Detailed field computations have been made with this program as well, including the configuration of the field at the ends and at the current contacts. A result of the field computation is given in reference 1.

The adiabatic temperature rise at the end of the pulse is shown in Figure 3. The temperature has peaks at the points of high current concentration, especially along the rim of the lithium. In the steel, however, it is highest in the corner where the current makes a U-bend.

More refined computations of the temperature rises have been made for the U-bend taking into account its detailed rounded shape. The maximum temperature rises are:

Steel:
- at rim of straight central section $\Delta T = 5.8$ °C
- in bend $\Delta T = 27.3$ °C

Lithium:
- at rim of straight central section $\Delta T = 45.7$ °C
- in bend $\Delta T = 56.0$ °C

The influence of the geometry on the temperature rise is more pronounced in the steel than in the lithium.

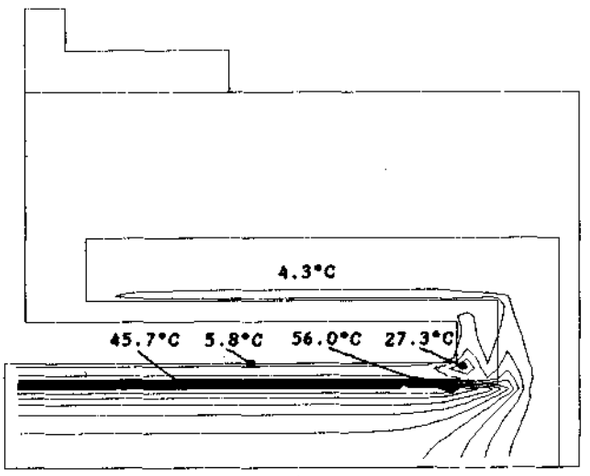

Fig. 3. The isotherms in the lens.

Current Concentration and Temperature Rise in the Current Contacts

The concentrations around the aluminium/steel current contacts, similar to the design described in reference 7, have been studied in more detail. The current distributions obtained are shown in Figures 4a, b, c and d, at the same instants as those of Figure 2. Although at the beginning the current is most concentrated at the left rim, it spreads sufficiently quickly through the aluminium such that, at peak current, most of the provided contact surface contributes to the current transfer. The maximum current densities on the mating face are 160 A/mm^2 at the left rim at 120 µsec. and 140 A/mm^2 at the right rim at 500 µsec which corresponds to respectively 250% and 220% of a uniformly distributed peak current. At the end of the pulse, current concentrations of opposite sign appear on each side of the contact (Figure 4d) with a zero current region in the centre. These eddy currents have practically vanished at 700µsec.

A larger contact surface would only then lead to a reduction of the current density if the electric resistivity of the contact materials would be increased accordingly to obtain a quicker diffusion.

Owing to the proper dimensioning of the contact pieces, the temperature rises per pulse are less than 2°C around the contacts.

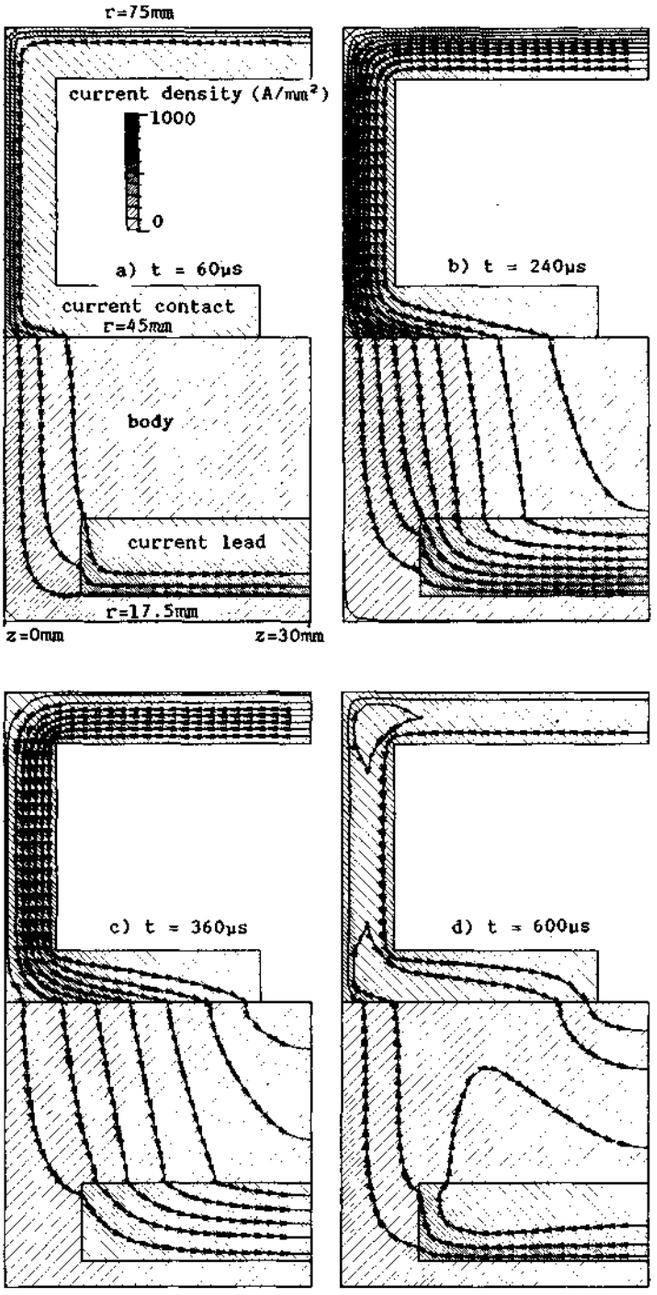

Fig. 4. The current flow at the cylindrical contact.

Lilthium Current Leads

The lithium current leads (see Figure 1) are meant to channel the current from the steel smoothly into the central lithium conductor. It is interesting to see whether a lens without such lithium leads, which obviously would be simpler to make, could be a valid alternative. In fact, the steel body, although a bad conductor, distributes the current so much faster that the overall resistance may very well come close to that of the lithium leads in which the current stays concentrated for quite some time. Calculations have been made for two of such simplified lens designs and Figures 6 and 7 show the current distributions at the working point. For comparison, Figure 5 (identical to Figure 2c) shows the current flow in the actual design. The temperature peaks in the lithium and in the steel, observed in the geometry of Figure 6 are not higher than those in the geometry shown in Figure 5. However, for the geometry of Figure 7, the temperature peak in the U-bend rises in the steel by about 70%.

These calculations indicate that considerable simplifications of the design should be feasible, which may however increase somewhat the overall resistance and inductance of the lens. On the other hand, the lithium leads in the present design act as a buffer volume which absorbs a substantial part of the thermal expansions of the strongly heated central part thus reducing the thermal stresses. Suppression of the buffer volume should therefore be considered with care.

Conclusion

The calculated current densities and temperatures of the CERN lithium lens show that the actual design is sound from the point of view of current distribution. The U-bend of the current at the end faces causes local current concentrations but these result in only small local temperature rises and optimisation of this bend is of little interest.

The aluminium current contacts around the steel housing are well dimensioned and current concentrations cause no important temperature rises.

The lithium current leads located inside the steel housing, designed for a smooth current transfer from the steel body into the lithium and finally into the central conductor could eventually be disposed of in favour of a simpler design, but at the expense of a reduced buffer volume which is useful for the reduction of the thermal stresses in the central part of the steel body.

References

1. R. Bellone, A. Ijspeert, P. Sievers, Contribution to this conference.
2. P. Sievers, R. Bellone, A. Ijspeert, P. Zanasco, IEEE Trans. on Nucl. Sci., Vol. 32 (1985), 3066-3068.
3. A. Ijspeert, P. Sievers, CERN SPS/85-10 (ABT), 1985.
4. A. Lennox, pbar Note 269, Fermilab, 1983.
5. R. M. Polivka, E. L. Wilson, University of California, 1976.
6. A. Ijspeert, P. Sievers, CERN/SPS/ABT/AI/BC/ Tech. Note 86-2, 1986.
7. G. Dugan, et al. IEEE Trans. on Nucl. Sci., Vol. NS-30, 4, 3660 (1983).

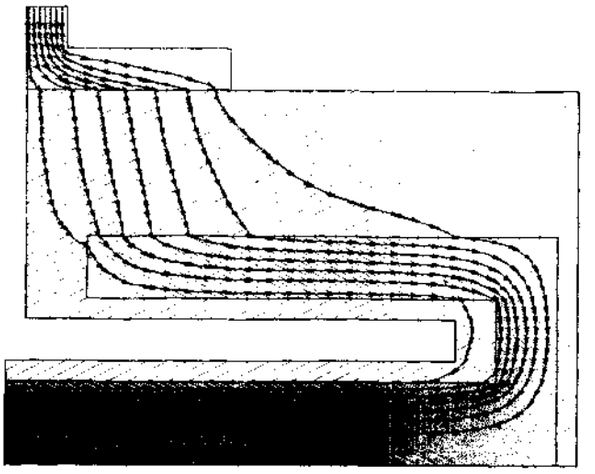

Fig. 5. The current flow in the lithium lens at 360 µsec. (identical to Figure 2c)

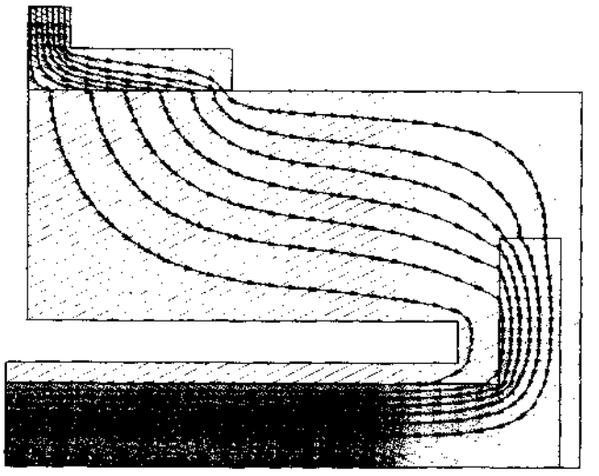

Fig. 6. The current flow in a simplified geometry at 360 µsee. (Variant 1).

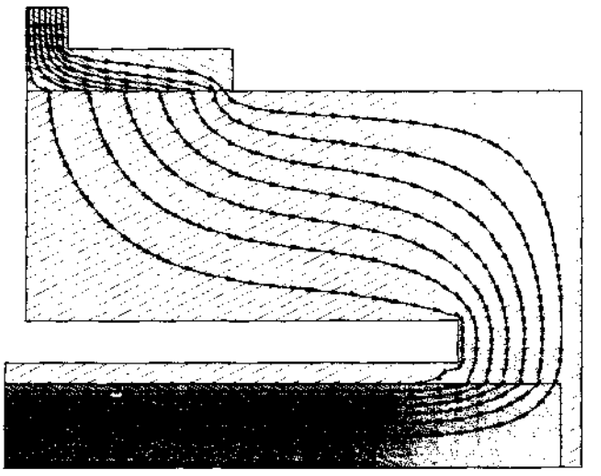

Fig. 7. The current flow in a simplified geometry at 360 µsec. (Variant 2).